scientific reports

Check for updates

OPEN

Facile fabrication of screen-printed MoS_2 electrodes for electrochemical sensing of dopamine

Michaela Pavličková[1], Lenka Lorencová[2], Michal Hatala[1], Miroslav Kováč[1], Ján Tkáč[2] & Pavol Gemeiner[1]✉

Molybdenum disulfide (MoS_2) screen-printed working electrodes were developed for dopamine (DA) electrochemical sensing. MoS_2 working electrodes were prepared from high viscosity screen-printable inks containing various concentrations and sizes of MoS_2 particles and ethylcellulose binder. Rheological properties of MoS_2 inks and their suitability for screen-printing were analyzed by viscosity curve, screen-printing simulation and oscillatory modulus. MoS_2 inks were screen-printed onto conductive FTO (Fluorine-doped Tin Oxide) substrates. Optical microscopy and scanning electron microscopy with energy-dispersive X-ray spectroscopy (SEM/EDX) analysis were used to characterize the homogeneity, topography and thickness of the screen-printed MoS_2 electrodes. The electrochemical performance was assessed through differential pulse voltammetry. Results showed an extensive linear detection of dopamine from 1 µM to 300 µM ($R^2 = 0.996$, sensitivity of 5.00×10^{-8} A µM^{-1}), with the best limit of detection being 246 nM. This work demonstrated the possibility of simple, low-cost and rapid preparation of high viscosity MoS_2 ink and their use to produce screen-printed FTO/MoS_2 electrodes for dopamine detection.

Two-dimensional (2D) nanomaterials have received attention in the field of chemistry, material science, physics, and nanotechnology after the successful exfoliation of graphene from graphite using Scotch tape in 2004 by Novoselov et al.[1,2]. 2D nanomaterials are defined as a class of freestanding sheet-like nanomaterials. They all have a thickness of merely a single or few atomic layers[3,4]. There has been a great effort to develop various 2D nanomaterials in recent years because of their unique properties, such as a large surface area, high chemical stability, high conductivity, mechanical strength, and optical transparency[5,6]. These materials include transition metal carbides, nitrides and carbonitrides (MXenes), hexagonal boron nitride (h-BN), graphene oxide (GO), transition metal dichalcogenides (TMDs) and many more[3,6].

Molybdenum disulfide (MoS_2) belongs to a class of materials called transition metal dichalcogenides (TMDs)[7]. It has a 2D layered structure where layers of Mo atoms are positioned between layers of S atoms. A strong covalent bond holds Mo-S layers while weak Van der Waals interaction exists between S layers[8,9]. MoS_2, because of its excellent properties, such as flexibility, photoluminescence, direct bandgap (~ 1.9 eV), excellent catalytic activity and biocompatibility, can be used for applications in catalysis, transistors, energy storage and sensor devices[9–11]. Moreover, MoS_2 has been successfully used to detect small molecules, *e.g.* hydrogen peroxide, glucose, eugenol, ascorbic acid, uric acid and dopamine[7,10,12].

Dopamine (DA) is a hormone and neurotransmitter regulating the function of human metabolism, immune, hormonal, central nervous and cardiovascular systems in the human brain[10,13]. The deficiency of DA can lead to various neurological diseases, *e.g.* schizophrenia, Alzheimer's and Parkinson's disease. Hence, determining the DA concentrations is beneficial for disease diagnosis[7,14].

Standard sensors for detecting various analytes are commonly prepared by modifying commercial screen-printed carbon electrodes (SPCE). This step is usually performed by various coating techniques[7,15,16], especially the drop-casting method[7,10,14,17]. Drop-casting is a convenient, facile technique that requires simpler and less expensive equipment, and the applied inks do not have prescribed physical and rheological properties and

[1]Department of Graphic Arts Technology and Applied Photochemistry, Faculty of Chemical and Food Technology, Slovak University of Technology in Bratislava, Radlinského 9, 812 37 Bratislava, Slovak Republic. [2]Institute of Chemistry, Slovak Academy of Sciences, Dúbravská cesta 9, 845 38 Bratislava, Slovak Republic. ✉email: pavol.gemeiner@stuba.sk

chemical formulation[18,19]. However, it has several disadvantages, *e.g.* low reproducibility and uncontrollable distribution of the deposited material[18]. Low-viscous dispersions used for the drop-casting method have to contain suitable solvents, *e.g.* dimethylformamide (DMF)[7], deionized water[20] or *N*-metylpyrolidon (NMP)[21]. Ultrasonication and centrifugation are used for dispergation and to eliminate or reduce the unexfoliated flakes [22]. In contrast, printing techniques (screen-printing) have high reproducibility and the possibility to prepare various fine structures for a wide range of layer thicknesses[18]. Also, the inks can be printed onto rigid or flexible substrates, and it is a low-cost, simple manufacturing process used for diverse applications[23].

MoS_2 sensors for dopamine detection prepared by modifying commercial screen-printed carbon electrode (SPCE) or glassy carbon electrode (GCE) have shown a low limit of detection (LOD)[7,17]. Zribi et al. modified SPCE by MoS_2 dispersion. The MoS_2 dispersion was prepared by ultrasonication of MoS_2 powder in a sodium cholate water solution. They used the drop-casting method for modification and achieved LOD of 0.085 μM[17]. Moreover, many researchers combine MoS_2 inks with graphitic materials, *e.g.* graphene[14], graphitic carbon nitride[13], graphene oxide (GO)[13,15] or metals, such as Ag[10,16]. Importantly, these materials have good conductivity and can detect dopamine at low concentrations[16]. Cheng et al. prepared a highly sensitive electrochemical sensor with LOD of 0.007 μM constructed by modifying GCE by graphene-MoS_2 inks[14]. Sookhakian et al. prepared Ag@MoS_2-modified GCE with excellent selectivity, high sensitivity and a low LOD of 0.2 μM[10]. In all previously mentioned cases, the GCE was modified by the drop-casting method.

Rowley-Neale et al. prepared screen-printable carbon/MoS_2 inks as a mixture of commercially available carbon ink and MoS_2 powder. Their screen-printed carbon/MoS_2 working electrodes were successfully used for electrochemical investigation of oxygen reduction reaction (ORR)[18].

Herein, screen-printable and highly viscous MoS_2 inks were prepared by mixing MoS_2 with various particle sizes and an ethylcellulose binder. Inks were screen-printed onto conductive FTO (Fluorine-doped Tin Oxide) substrates. The suitability of prepared MoS_2 inks for screen-printing was evaluated by rheological behavior analysis. The homogeneity, topography and thickness of layers were analyzed by optical microscopy and scanning electron microscopy with energy-dispersive X-ray spectroscopy (SEM/EDX) analysis. Finally, the functionality of the electrodes was studied by electrochemical measurements. This work aims at the fast and simple preparation of printable high viscosity MoS_2 inks, which can be used to fabricate screen-printed FTO/MoS_2 sensors for dopamine detection at a submicromolar level. To our best knowledge, this is the first screen-printed sensor based on MoS_2 nanomaterial for the detection of dopamine.

Experimental section

Materials. Molybdenum disulfide (MoS_2) powder with particle size of ~ 6 μm (max. 40 μm), molybdenum disulfide (MoS_2) nanopowder with particle size of 90 nm, ethylcellulose (EC) (viscosity 22 cP 5% in toluene/ethanol 80:20), terpineol (≥ 96%, bp 213 °C) and FTO (Fluorine-doped Tin Oxide, 7 Ω/sq) glass substrates were purchased from Sigma Aldrich. Dopamine hydrochloride (DA, $C_8H_{11}NO_2$.HCl) and phosphate buffer (PB) components (KH_2PO_4 and K_2HPO_4, pH 7.0) used for electrochemical analysis were also ordered from Sigma Aldrich. All solutions were freshly prepared in ultrapure deionized water (0.055 μS cm^{-1}).

MoS_2 inks preparation. First, the polymeric binder was prepared by dissolving 8 wt% (EC) in terpineol. After that, MoS_2/EC inks were prepared by dispersing 25, 45 and 60 wt% of MoS_2 powder with particle size of ~ 6 μm (max. 40 μm) in a polymeric binder (samples Mo6-25; Mo6-45 and Mo6-60). In the case of MoS_2 nanopowder with particle size of 90 nm, only inks with 25 and 45 wt% of MoS_2 (samples Mo90-25 and Mo90-45) were prepared. Inks with 90 nm particle content over 45 wt% were not miscible. All inks were homogenized in a "homemade" hand-held mixing unit 5 times for 30 s.

Screen-printing process. The MoS_2 inks were screen-printed onto glass substrates covered by a conductive FTO layer. Before printing, FTO substrates were gradually pretreated in four steps; cleaning in detergent solution (1); acetone (2); isopropyl alcohol (3) in an ultrasonic bath, followed by UV-C treatment (4) for 20 min. For the screen-printing of prepared MoS_2 inks, yellow high modulus polyester yarn mesh was used, with mesh count 71 cm^{-1} and 48 μm thread diameter (PME 71–48 Y, SEFAR) in combination with the stencil prepared by the photochemical way. Screen-printed MoS_2 layers were prepared using a manual, auxiliary guide arm (constant pressure) equipped screen-printing machine (Screen Printing Table P65-80 KN, Drucktech). The printed area was 6 × 6 mm^2. After printing, MoS_2 layers were left for 10 min at laboratory temperature for levelling and then were dried in a laboratory oven at 120 °C for 30 min.

Characterization methods. The rheological properties of prepared MoS_2 inks were investigated using a rheometer (HAAKE, MARS iQ) equipped with parallel plate geometry with a diameter of 35 mm and a gap height of 0.4 mm. The temperature was set to 25 °C during all measurements. The steady-state rheological test was performed at shear rates [$\dot{\gamma}(s^{-1})$] of 0.001–1000 s^{-1} to measure the dynamic viscosity [η (Pa.s)] and was obtained by controlling shear rates (CR). The time-dependent controlled-shear-rate tests were performed to simulate the screen-printing process with constant shear rates in three intervals: (1) 0.5 s^{-1} for 90 s; (2) 1,000 s^{-1} for 30 s and (3) 0.5 s^{-1} for 180 s. The oscillatory tests are helpful to understand the structural changes of the inks occurring in the screen-printing process. In the shear strain amplitude sweep, the applied shear strain ranged from 0.1 to 100% at a frequency of 1 Hz, which helped to characterize the viscoelastic behavior of the inks and determine the linear viscoelastic region (LVR). Elastic and storage moduli were measured as a function of shear strain/stress. The elastic or storage modulus (G') is related to the ability of ink to store energy and represents the elastic portion of the viscoelastic behavior. The viscous or loss modulus (G'') indicates the fluidity of ink[24]. The

factor tanδ, which is G''/G' gives an indication of material internal strength and helps to define viscoelasticity (Eq. (1))[25].

$$tan\delta = G''/G' \tag{1}$$

The thicknesses of screen-printed MoS_2 layers were analyzed by optical microscope (LEICA DM 2700 M) using the 3D image sequential recording method. The software (Leica Application Suite V4, LEICA) was used to evaluate the arithmetic average of thickness. The adhesion of printed MoS_2 layers to FTO substrates was tested by peel adhesion test using the adhesive tape (Scotch Crystal, 3M). Disturbance of the screen-printed layers after peeling off the adhesive tape was evaluated. The layers were backlit from below, and the images were made by optical microscopy. The topography and homogeneity of FTO/MoS_2 layers were characterized by scanning electron microscopy with energy-dispersive X-ray spectroscopy (SEM/EDX; JEOL JSM-IT500HR). The electron acceleration voltage was set to 20 kV.

All procedures for evaluation of the performance of FTO/MoS_2 electrodes for electrochemical sensing were run with a laboratory potentiostat/galvanostat Autolab PGSTAT 302 N with an impedimetric module (Ecochemie, Utrecht, Netherlands) in combination with NOVA 1.10 software. Differential pulse voltammetry (DPV) was used for the detection of dopamine. MoS_2 layers onto FTO substrates were used as working electrodes, the platinum wire was used as the counter-electrode and an argentochloride electrode (Ag/AgCl/3 M KCl) as the reference electrode. Five scans were run in a plain phosphate buffer pH 7.0 in a potential window of 0–1 V to stabilize FTO/MoS_2 electrodes. The parameters applied for the differential pulse voltammetry were as follows: 50 ms modulation time, 0.5 s interval time, 25 mV modulation amplitude, and 5 mV step. Measurements were run under Nova Software 1.10, and data acquired were evaluated using OriginPro 9.1. The limit of detection (LOD) was calculated as a signal-to-noise ratio (S/N) = 3.

Result and discussion

In order to investigate the influence of ink formulation on rheological properties, different screen-printable MoS_2 inks were prepared with various particle sizes and concentrations of MoS_2. All prepared MoS_2 inks exhibited typical shear-thinning non-Newtonian rheological behavior (Fig. 1a). It is characterized by a decreasing dynamic viscosity with an increasing shear rate, and it is crucial for the screen-printing process[24]. The increasing shear rate adversely affects the cohesive internal forces between the particles and the binder and destroys the ink structure, which leads to an unsteady ink system[26]. When the shear rate increased from 0.001 to 1000 s^{-1}, the dynamic viscosity of all inks dropped gradually. It is obvious that dynamic viscosity increases with MoS_2 concentration. The viscosity of Mo6-60 sample with the highest MoS_2 content was slightly higher than what would be optimum for screen-printing. The maximum value was 105 Pa.s at 10 s^{-1}, and the minimum value was 0.02 Pa.s at 1000 s^{-1}. This rapid decrease indicates that a higher concentration of MoS_2 causes a faster breakdown of the structure. It is also clear that particle size does not significantly affect dynamic viscosity. Values of dynamic viscosity are identical (the maximum was ~ 9 Pa.s and the minimum was 3 Pa.s) for samples Mo6-25 (particle size ~ 6 µm) and Mo90-25 (particle size ~ 90 nm) containing 25 wt% of MoS_2. The same values (the maximum was ~ 22 Pa.s and the minimum was ~ 2 Pa.s) were obtained also for samples Mo6-45 (particle size ~ 6 µm) and Mo90-45 (particle size ~ 90 nm) containing 45 wt% of MoS_2.

The viscosity of screen-printable inks has to be low enough (under applied external force) to allow the squeegee to press the ink through the screen mesh, but also high enough (after releasing the force) to support ink to retain the geometry of printed patterns[24]. The rheological behavior of MoS_2 inks during the screen-printing process simulated by the time-dependent controlled-shear-rate tests is shown in Fig. 1b, and the characteristic parameters are listed in Supplementary Table S1. Screen-printing process can be divided into three steps. The first interval of the curve simulates the behavior of the ink at rest on the screen at a pre-set low shear rate (0.5 s^{-1} for 90 s). The second interval corresponds to the structural breakdown of the ink when it is pressing through the openings in the screen. The shear rate increases up to 1000 s^{-1} for 30 s. Finally, in the third interval, the shear rate decreases to 0.5 s^{-1} for 120 s to allow structural regeneration evaluation. During the shear rate increase from 0.5 to 1000 s^{-1} in the second interval, the viscosity value drops significantly (Fig. 1b and Supplementary Tab. S1). The applied shear stress destroys the internal structure of the inks. Subsequently, the ink structure is rebuilt and restored when the shear rate returns to 0.5 s^{-1} in the third interval[26]. The viscosity of Mo6-25 and Mo90-25 was the lowest (8.8 and 8.9 Pa.s) at 0.5 s^{-1}, and these samples showed the highest recovery rate of 97% and 94% in 250 s, respectively. In addition, the rheological behavior during the process of the screen-printing simulation was the same for samples containing 25 wt% of MoS_2 (Mo6-25, Mo90-25) and also for the samples containing 45 wt% of MoS_2 (Mo6-45, Mo90-45). Thus, the particle size does not have a noticeable effect on the printing paste rheology within the printing process. The regeneration of these four samples was quick from the beginning, with the rise of the curve being slow afterwards. The recovery rate of sample Mo90-45 is slightly over 100% in 250 s (Fig. 1b). Thus, if the third interval was longer, viscosity would drop back to (or even under) the reference value[27]. The result of the screen-printing simulation process for the sample Mo6-60 is different from the samples with lower MoS_2 concentrations. The initial viscosity is too high (170 Pa.s), and as the shear rate increased to 1000 s^{-1}, the viscosity decreased to 2.5 Pa.s. In the third interval, the regeneration is slower, indicating a longer time for levelling of the applied layers after printing, resulting in a smoother surface. Despite the recovery rate being only 60%, due to the slower increase in viscosity during the regeneration step, sample Mo6-60 can be considered the most suitable from a layer topography point of view.

To investigate the impact of MoS_2 concentration and particle size on the viscoelastic properties of the inks, oscillatory measurements were carried out for prepared inks, specifically shear strain amplitude sweep tests. Figure 1c shows the storage (G') and loss modulus (G'') dependences of prepared MoS_2 inks at shear strain varying from 0.1 to 100%. The curve shapes of the samples with the same concentration of MoS_2 (samples Mo6-25 and

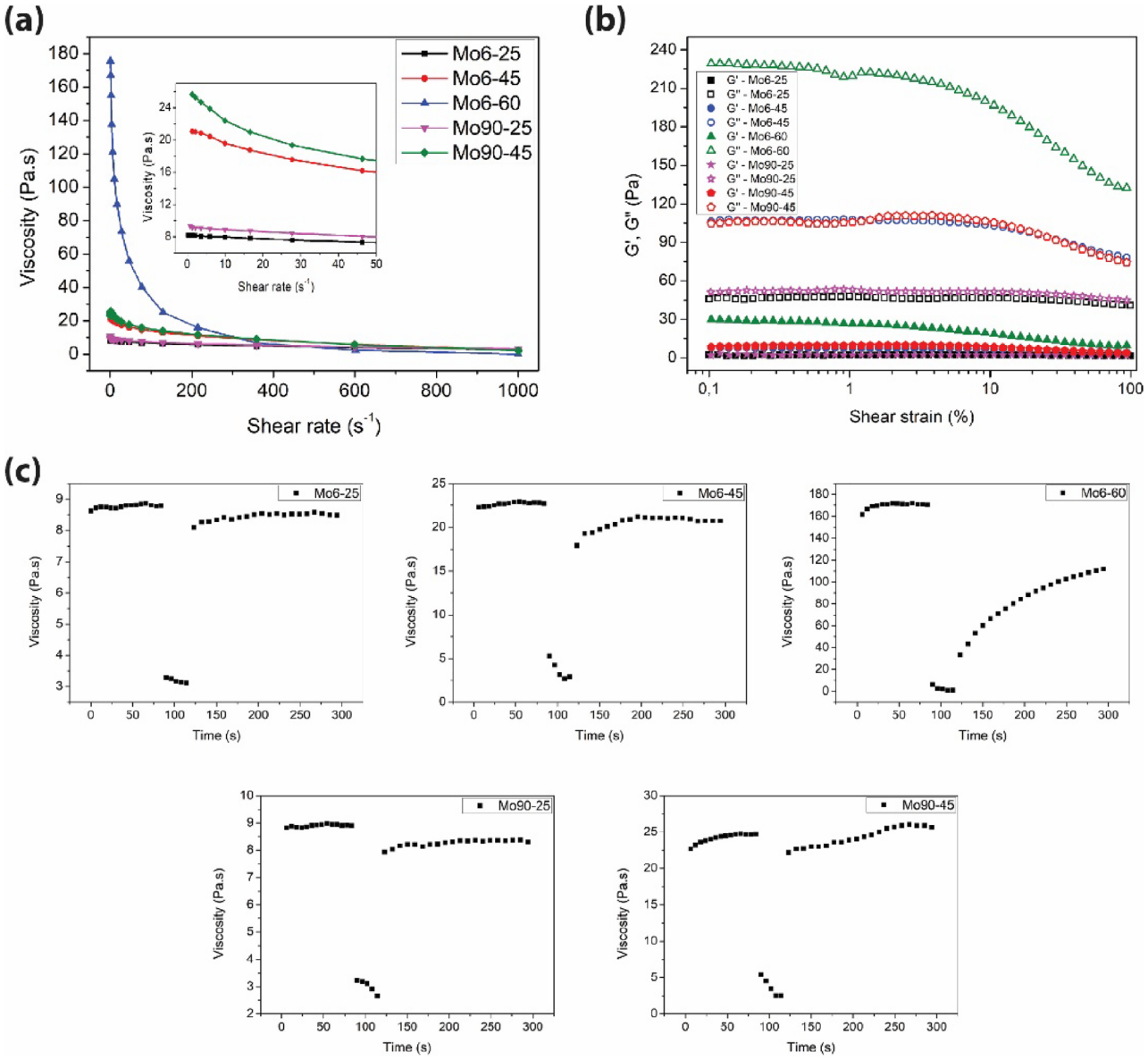

Figure 1. (**a**) Dynamic viscosity of screen-printable MoS_2 inks at shear rates ranging from 0.01 to 1,000 s^{-1}. (**b**) Shear strain sweep of MoS_2 inks. (**c**) Rheological behavior of MoS_2 inks during simulation of screen-printing.

Sample	LVR end point (%)	G' at LVR end point (Pa)	G'' at LVR end point (Pa)	G''/G' at LVR end point
Mo6-25	41.11	2.16	43.83	20.29
Mo6-45	10.88	7.56	103.81	13.73
Mo6-60	1.65	28.76	222.37	7.73
Mo90-25	34.73	2.44	51.66	21.17
Mo90-45	9.01	9.59	90.19	9.40

Table 1. The oscillatory strain sweep parameters in the LVR.

Mo90-25; samples Mo6-45 and Mo90-45) are similar even though they had different particle sizes. The oscillatory test results (values of LVR, G' and G'') for MoS_2 inks are listed in Table 1.

The LVR is defined as the region in which the ink can endure mechanical deformation without destroying the structure[28]. LVR values are determined from the G' curves. Beyond the LVR, the values of G' and G'' are continuously decreasing for all samples, indicating the gradual internal structure breakdown. The highest LVR had samples containing 25 wt% of MoS_2 (< 42%), followed by samples with 45 wt% of MoS_2 (< 11%), and the lowest

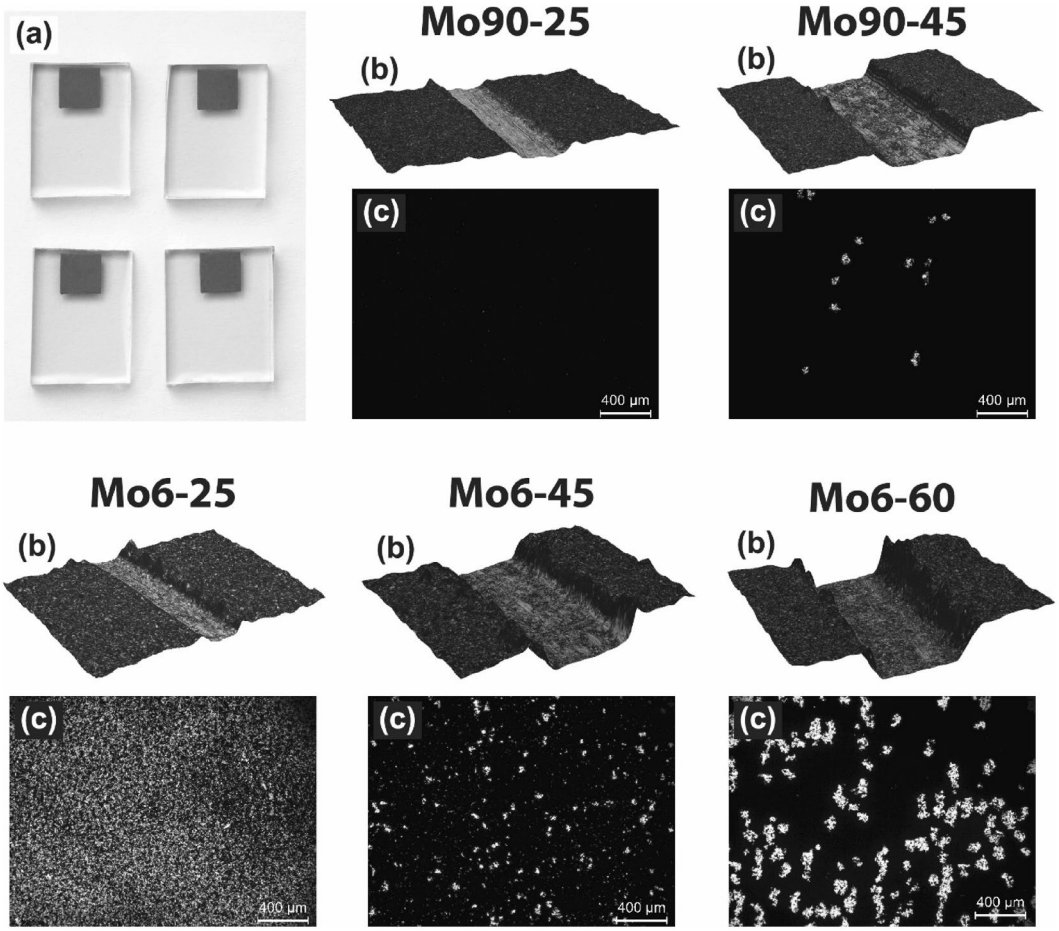

Figure 2. (**a**) Screen-printed MoS_2 layers onto FTO substrates. (**b**) Needle scratch was made through the middle of the MoS_2 layers, and the thickness measurement was evaluated by an optical microscope using the 3D image sequential recording method. (**c**) Optical microscopy images of MoS_2 layers after the peeling test evaluated adhesion to FTO substrates.

LVR had a sample with 60 wt% of MoS_2 (< 2%). All samples show liquid behavior ($G'' > G'$) across the entire strain amplitude range. From Table 1, the G' increase with MoS_2 concentration, measured values for Mo6-25, Mo90-25, Mo6-45, Mo90-45 and Mo6-60 are 2.16, 2.44, 7.56, 9.59 and 28.76, respectively. Further investigation of the inks elastic behavior was carried out by analyzing the ratio of liquid-like to solid-like bahavior (G''/G') , the loss factor—tanδ within the LVR (Table 1). A tanδ < 1 demonstrates that the ink is elastic, cohesive or tacky[26]. All prepared MoS_2 inks have a loss factor tanδ > 1, which indicates viscous behavior[24]. Decreasing loss factor tanδ within the LVR indicates that the MoS_2 content can positively impact the inks' structural strength and elasticity[29].

After rheology characterization, MoS_2 inks were screen-printed onto FTO substrates (Fig. 2a). The thickness of MoS_2 electrodes was evaluated for layers screen-printed onto Al_2O_3 ceramic substrates. These substrates were chosen because of their smooth surface, opacity and, from our experience, are more suitable for thin layer thickness measurements. First, a needle scratch was made through the middle of the layers. After that, thicknesses were evaluated by optical microscope using the 3D image sequential recording method (Fig. 2b). As expected, the thickness increased with the concentration of MoS_2 in the inks, and the measured values ranged from 4 ± 1 to 18 ± 1 µm. Specifically, measured values were 4 ± 1, 11 ± 2 and 18 ± 1 µm for samples Mo6-25, Mo6-45, Mo6-60 and 4 ± 1, 10 ± 1 µm for Mo90-25 and Mo90-45, respectively. As it was seen, particle size did not influence the thickness, but layers based on smaller 90 nm MoS_2 particles had lower roughness.

Screen-printed MoS_2 layers have undergone an evaluation of adhesion to FTO substrate by a peeling test. Figure 2c shows optical microscopy images of samples after the peeling test. As it can be seen, layers containing 6 µm MoS_2 have lower adhesion than layers containing 90 nm MoS_2. Also, a more significant part of the layer was pulled down with increasing MoS_2 concentration. Therefore, the highest adhesion to FTO substrate was evaluated for the sample based on 90 nm MoS_2 with the lowest particle content (Mo90-25). The adhesion to the FTO substrate and the cohesion of the layers are mainly affected by the size of the particle's phase interface, their surface energy, and the concentration of ethylcellulose. Therefore, the degree of adhesion could be increased by finding the ideal ratio between binder, ethylcellulose, and MoS_2.

SEM measurements showed (Supplementary Fig. S1) that the particle size in the layers prepared from MoS_2 particles, characterized by the manufacturer as particles with an average size of 90 nm, actually ranged up to

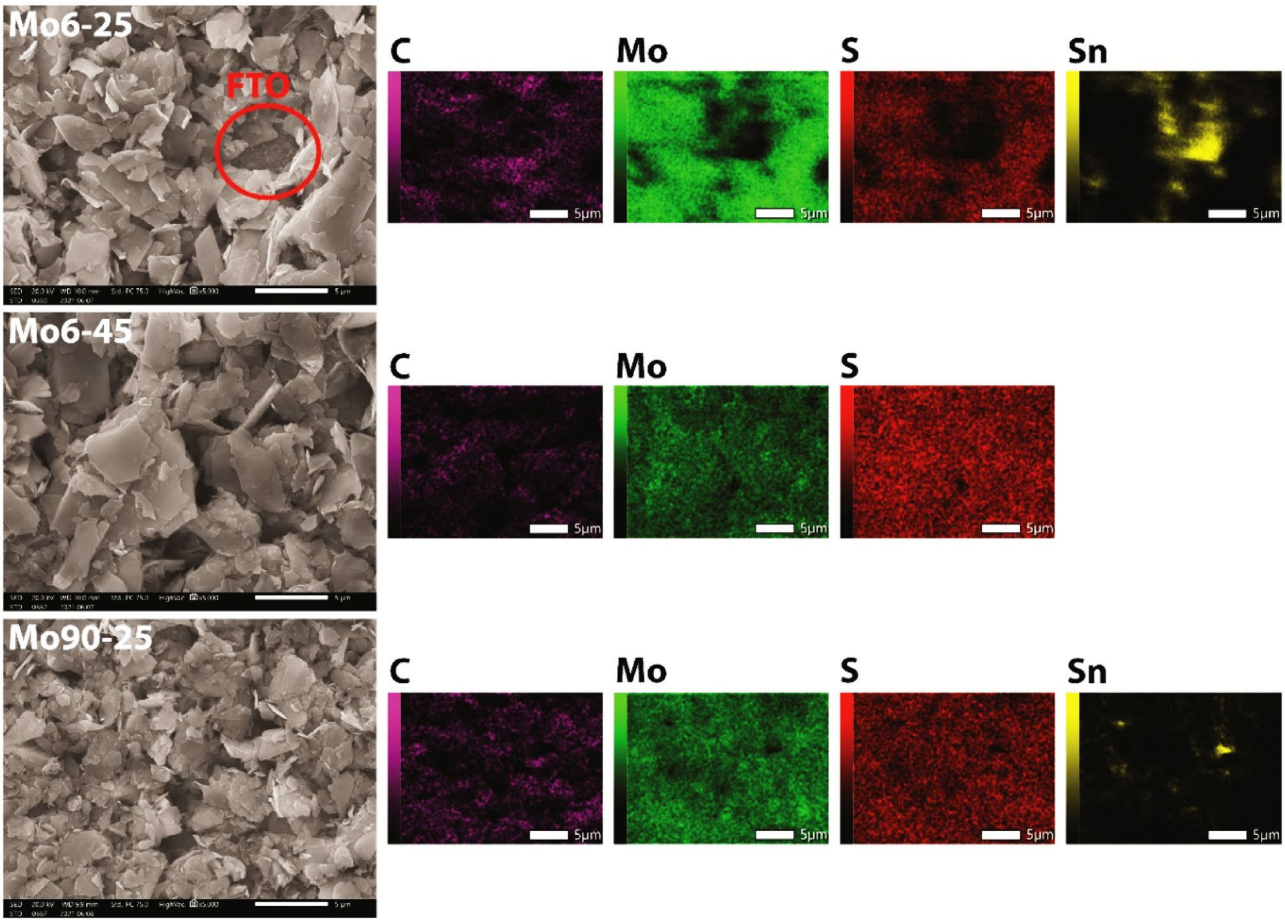

Figure 3. SEM/EDX analysis of printed Mo6-25, Mo6-45 and Mo90-25 layers.

micrometres. Therefore, we assume that the manufacturer's labelling refers more likely to the particles with the highest frequency of occurrence (90 nm) than their average size. Despite the discrepancy, it was evident from the SEM measurements that the average diameter of particles referred to as 90 nm is lower than the diameter of the second particle type used with a more correctly declared average size of 6 µm (Supplementary Fig. S1). In addition, similar to the layer thickness measurements, it is evident that the layers prepared from the 90 nm MoS_2 inks have a smoother surface, with a higher frequency of submicron particles. Figure 3 shows SEM and EDX mapping results of selected samples Mo6-25, Mo6-45 and Mo90-25. The homogeneity of printed electrodes was insufficient in the case of the lowest MoS_2 concentrations, regardless of the particle size (Mo6-25 and Mo90-25). As a result, these electrodes did not cover FTO substrates homogenously, as shown in the SEM images or EDX element maps (measured Sn signal from the FTO). Insufficient homogeneity of these MoS_2 electrodes, related to the measured lowest thickness of 4 µm, can be problematic when applied to electrodes other than FTO. For example, when applied onto Ag electrodes in printed three-electrode systems, which are primarily intended to provide electron transport from the working electrode and can not interact with the analyte solution. Printed electrodes with 45 wt% and 60 wt% MoS_2 were homogenous and did not expose the surface of FTO substrates. Supplementary Tab. S2 shows the atomic representation of the detected elements, where the carbon intensity corresponds to the added binder ethylcellulose and varies depending on its concentration.

Electrochemical detection of dopamine by applying screen-printed FTO/MoS_2 electrodes. Electrochemical performance of fabricated FTO/MoS_2 working electrodes was first evaluated in 0.1 M PB of pH 7.0, employing cyclic voltammetry (CV). Figure 4 shows representative cyclic voltammograms resulting from runs at conductive FTO substrates modified with MoS_2 in a potential window from − 0.5 V to 0.8 V at a sweep rate of 100 mV s^{-1}. Electrochemical investigation of FTO/MoS_2 electrodes, *i.e.* FTO/Mo6-25, FTO/Mo6-45, FTO/Mo6-60, FTO/Mo90-25 and FTO/Mo90-45, in a plain electrolyte revealed that there were no so significant differences in the capacitive current response between screen-printed FTO/MoS_2 electrodes (Fig. 4).

Dopamine molecule plays an important role in human metabolism, being a crucial neurotransmitter in the central nervous system maintaining neuro-physiological control of mental activities. The concentration of DA ranges between 1 and 2 mM in the intracellular fluids of the central nervous system. Any relevant deviation from an optimal concentration of dopamine in the body causes Parkinson's disease or schizophrenia. Since dopamine is electrochemically active, it may be detected by electrochemical oxidation.

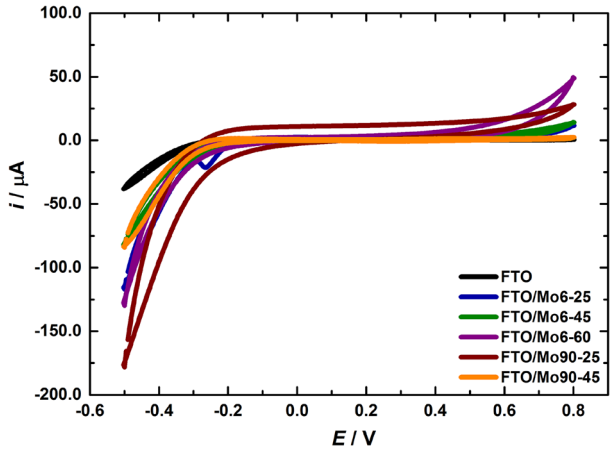

Figure 4. Cyclic voltammograms recorded for screen-printed FTO/MoS_2 electrodes, *i.e.* FTO/Mo6-25, FTO/Mo6-45, FTO/Mo6-60, FTO/Mo90-25 and FTO/Mo90-45, respectively in a potential window of – 0.5 V–0.8 V at a scan rate of 100 mV s^{-1}, 20th cycles. Electrolyte: 0.1 M PB pH 7.0.

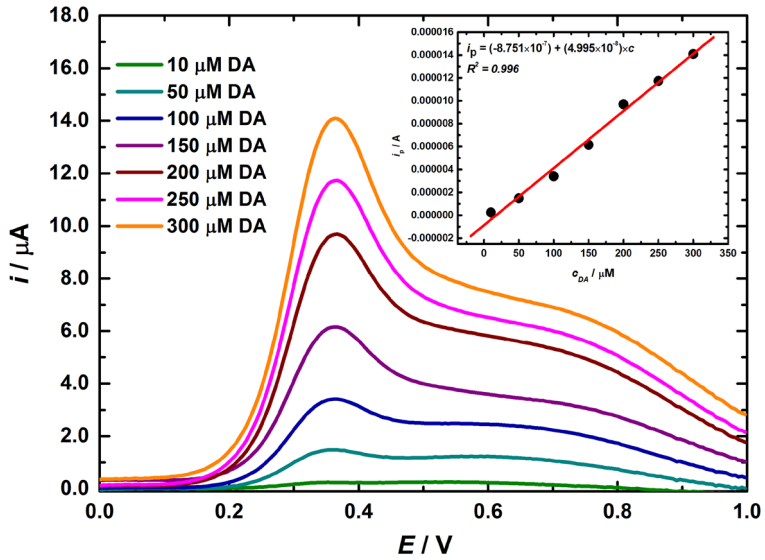

Figure 5. Background-subtracted differential pulse voltammograms obtained for various concentrations of dopamine (DA) at sample FTO/Mo6-45. Electrolyte: 0.1 M PB pH 7.0. Inset figure shows a calibration curve.

The electrochemical behaviour of screen-printed FTO/MoS_2 electrodes, i.e. FTO/Mo6-25, FTO/Mo6-45, FTO/Mo6-60, FTO/Mo90-25 and FTO/Mo90-45, was assessed by DPV experiment. The DPV curve of sample FTO/Mo6-45 showing electrochemical oxidation of dopamine in 0.1 M phosphate buffer (pH 7.0) as a supporting electrolyte can be clearly seen in Fig. 5. The DPV curves of other samples are shown in Supplementary Fig. S2. The linear dependence of i_p (oxidation peak current) vs. c_{DA} (concentration of dopamine) was investigated in the range up to 300 µM for the measured target analyte. The limit of detection (LOD) was calculated according to S/N = 3. The best LOD value of 246 nM ($R^2 = 0.996$) was calculated for the Mo6-45 sample with sensitivity of 5.00×10^{-8} A μM^{-1}. The other modified electrodes exhibited the following LODs: 456 nM ($R^2 = 0.982$) for Mo90-25, 669 nM ($R^2 = 0.975$) for Mo6-60, 686 nM ($R^2 = 0.995$) for Mo6-25 and 865 nM ($R^2 = 0.976$) for the Mo90-45 sample. The response towards 10 mM DA was 245 nA on an electrode modified by Mo6-45 ink, while a significantly lower response of 45 nA was observed on a bare FTO electrode.

MoS_2 has been studied as a working electrode material for DA detection in many works by various authors. However, most of this work is devoted to sophisticated MoS_2 electrodes modified with other materials and prepared by different techniques, which are not as suitable for mass production of working electrodes as printing. Moreover, printing (especially screen-printing) brings several advantages, such as simple, cheap, fast and reproducible preparation of electrodes in large areas on various and flexible substrates. Below, for comparison, are briefly mentioned works of other authors dealing with the preparation of MoS_2 sensors for DA detection

Electrode platform	Modification of sensing surface area	Detection technique	LOD obtained for DA determination (μM)	Linear range (μM)	Deposition technique	References
GCE	Self-assembled AuNPs@ MoS_2-NSs	CV	1.0	5.0–200.0	Drop-casting	Zou et al.[35]
GCE	MoS_2@MB nanohybrid	DPV	0.58	1.0–500.0	Modifying GCE by MoS_2@MB film	Su et al.[30]
GCE	MoS_2-RGO BC_5N	DPV	MoS_2-Gr/GCE: 0.55 BCN/GCE: 2.1	MoS_2-RGO: 1–110 BCN/GCE: 2.3–20	Drop-casting	Pramoda et al.[31]
-	3D Ni/NiO/MoS_2/rGO foam	CV	0.09	0–3	Hydro-thermal method/ Electro-deposition	Zhang et al.[32]
CPE	MoS_2/Au	DPV	76×10^{-3}	0.5–300	Drop-casting	Chen et al.[36]
rGO/ITO	MoS_2 – GCN	PEC sensor	1.6×10^{-3}	0.005 – 1271.93	Drop-casting	Velmurugan and Yang[13]
CC	MoS_2NS	CV	0.30	250–4000	Growth of MoS_2 on CC	Sabar et al.[40]
GCE	AuNPs@MoS_2	DPV	0.05	0.05–30	Drop-casting	Sun et al.[45]
CNFs	MoS_2-NSBs	DPV	36×10^{-3}	1–60	Hydro-thermal method	Yue et al.[37]
GCE	3D-f-MoS_2-rGO	DPV	0.05	0.2–150	Drop-casting	Ma et al.[33]
GCE	3D-MoS_2/rGO/Au	DPV	0.11; in a mixture: 0.15	0.5–140.5; in a mixture: 0.3–204.3	Drop-casting	Zhao et al.[38]
GCE	MoS_2/PEDOT	DPV	0.52	1–80	Electro-deposition	Li et al.[41]
GCE	GNS-CNTs/MoS_2	DPV	50×10^{-3}	100×10^{-3} -100	Drop-casting	Mani et al.[46]
CP	MoS_2-R /Nafion:TBAB-Lac (*P. sanguineus*)	Amp	10×10^{-3}	0.1–0.5 1–5	Drop-casting	Rubio-Govea et al.[42]
CPE	Ms-atCNTs (p-Aln/Ms-atCNT)	DPV	0.08	0.6–45	Electro-polymerization	Kumar et al.[34]
ITO	Ag/MoS_2	Amp	0.20	0.2–50	Spin-coating	Shin et al.[16]
SPCE	2D-MoS_2	LSV	0.09	1–100	Drop-casting	Zribi et al.[17]
GCE	MoS_2-CPtNPs	DPV	0.11	1–500	Drop-casting	Zhu et al.[39]
ITO	MoS_2 NFs-rGO	DPV	0.12	5–60	Spray-coating	Guo et al.[15]
PGSs	Mn-doped MoS_2	DPV	5×10^{-3} in 10% serum	5×10^{-3} to 5	Drop-casting	Lei et al.[43]
GCE	pGr-MoS_2	CV	0.01×10^{-3}	0.00001–10	Drop-casting	Arya Nair et al.[47]
GCE	MoS_2NS	ECL	8.5×10^{-4}	1.0×10^{-3}- 1.0×10^{-1}	Spreading on the working area	Zhang et al.[44]
FTO	**MoS_2 (6 μm)**	**DPV**	**0.25**	**1–300**	**Screen-printing**	**This work**

Table 2. Comparison of analytical performance of various DA electrochemical sensors depending on sensing platform modification, detection and deposition technique. *Ag/MoS_2* Silver encapsulated MoS_2 hybrid nanoparticle, *Amp.* Amperometry, *AuNPs* Gold nanoparticles, *BC_5N* Borocarbonitride, *CC* Carbon cloth, *CV* Cyclic voltammetry, *CPE* Carbon paste electrode, *CP* Carbon paper, *DA* Dopamine, *ECL* Electrogenerated chemiluminescence, *GCE* Glassy carbon electrode, *GNS-CNTs/MoS_2* Molybdenum sulfide flowers placed on graphene nanosheets and multiwalled carbon nanotubes, *ITO* Indium tin oxide, *Lac (P. sanguineus)* Laccase isoforms (LacI and LacII) from a native strain of the white-rot fungi known as *Pycnoporus sanguineus*, CS43, *LSV* Linear sweep voltammetry, *MB* Methylene blue, *MoS_2-NSs* MoS_2 nanosheets, *MoS_2 – GCN* A molybdenum disulfide–graphitic carbon nitride, *MoS_2-NSBs* Molybdenum disulfide nanosheets resembling the shape of golf balls, *MoS_2-R* Molybdenum disulfide ribbons, *Ms-atCNTs* MoS_2/acid-treated MWCNTs composite, *MoS_2-CPtNPs* Clover-like platinum nanoparticle-supported MoS_2, *MoS_2 NFs-rGO* MoS_2 nanoflowers-reduced graphene oxide, *p-Aln* Polymerized alanine, *pGr* Pulverized graphite, *pGr-MoS_2* A graphene-molybdenum disulphide nanocomposite, *PEC* Photoelectrochemical sensor, *PGSs* Pyrolytic graphite sheets, *RGO* Reduced graphene oxide, *rGO/ITO* Reduced graphene oxide/indium tin oxide, *SPCE* Screen-printed carbon electrode, *TBAB* Tetrabutylammonium bromide, *3D-f-MoS_2-rGO* Worm-like and flower-like molybdenum disulfide (MoS_2) grown on reduced graphene oxide (rGO), *3D-MoS_2/rGO/Au* 3D-networked nanostructure composed of MoS_2, reduced graphene oxide and gold nanoparticles.

prepared by various methods and based on different, primarily composite MoS_2 sensing platforms. It is clear from the comparison that the screen-printed MoS_2 working electrodes achieve not a best but comparable LOD in DA detection.

The individual and simultaneous detection of DA with LOD of 0.58 μM was performed by applying the redox-active dye Methylene Blue (MB) grafted onto MoS_2 nanosheet surface (MoS_2@MB) via electrostatic and π-stacking interaction[30]. Velmurugan and Yang obtained LOD of 1.6 nM for DA employing a MoS_2 – graphitic carbon nitride (MoS_2 – GCN) p – n heterojunction stabilized reduced graphene oxide/indium tin oxide (rGO/ITO) photoelectrode[13]. Additionally, more papers were previously published describing DA sensors employing graphene or MWCNTs and MoS_2 composites[13,15,31–34]. Moreover, instead of carbon-based nanomaterials, metallic nanoparticles (Au, Ag, Pt) in combination with MoS_2 were successfully applied to develop sensitive DA sensors[16,35–39]. Sabar et al. constructed a flexible and economically viable electrochemical sensor for DA detection consisting of the carbon cloth (CC) as a host interface for direct growth of MoS_2NS via hydrothermal

methodology[40]. Golf ball-like MoS_2 nanosheet arrays (diameter of ~ 2 μm) deposited on carbon nanofibers (CNFs) proved excellent electrochemical properties for the detection of DA[37]. The MoS_2 nanosheets incorporated into poly(3,4-ethylenedioxythiophene) (PEDOT) by electrodeposition onto GCE formed a nanocomposite detecting DA with LOD of 0.52 μM[41]. The amperometric biosensor (CP-MoS_2-R-Nafion:TBAB-Lac) for DA detection was fabricated by the modification of the carbon paper electrode surface with MoS_2 in the form of ribbons (MoS_2-R) and flowers (MoS_2-F), coupled with the immobilization of laccase enzymes[42]. Instead of other types of electrodes, the disposable SPCE were patterned with 2D-MoS_2 to develop an electrochemical biosensor for detection of DA achieving a sensitivity value of 1044 μA mM^{-1} cm^{-2}[17]. Lei et al. fabricated an electrochemical DA sensor based on Mn-doped MoS_2 synthesized via a scalable two-step approach (with Mn ~ 2.15 at. %)[43]. Zhang with co-workers found out that while MoS_2 nanosheets catalyzed the electro-oxidation process of $Ru(bpy)_3^{2+}$ to generate $Ru(bpy)_3^{3+}$, DA inhibited the effect on electrogenerated chemiluminescence (ECL) intensity of $Ru(bpy)_3^{2+}$-MoS_2 nanosheets through the energy transfer process. LOD of 8.5×10^{-10} mol L^{-1} was obtained for DA[44]. All mentioned works are summarized in Table 2.

Conclusion

The screen-printed FTO/MoS_2 working electrodes for the electrochemical detection of dopamine were successfully prepared in this work for the first time. Screen-printable MoS_2 high viscosity inks contained MoS_2 with different particle sizes and concentrations, ethylcellulose and terpineol. The screen-printing simulation confirmed that MoS_2 inks are suitable for screen-printing process with corresponding flow behavior, and the viscosity recovery rate. Oscillatory modulus determined the linear viscoelastic region and helped to understand the solid- and liquid-like behavior of prepared MoS_2 inks during screen-printing. After rheological behavior analysis, MoS_2 inks were screen-printed onto FTO substrates. The differential pulse voltammetry measurements showed that the best limit of detection of 246 nM for DA (S/N = 3) was evaluated for the working electrode printed using the ink containing 45 wt% MoS_2 powder with an average particle size of 6 μm. Presented results showed that screen-printable MoS_2 inks could be prepared by a simple, time-efficient mixing process taking only a few minutes. Moreover, MoS_2 inks prepared in this way allow the fabrication of working electrodes for detection of dopamine or further target analytes by simple, low cost and for mass suitable screen-printing technique.

Data availability

All data generated or analyzed during this study are included in this published article.

Received: 12 April 2022; Accepted: 6 July 2022
Published online: 13 July 2022

References

1. Yang, Y., Deng, H. & Fu, Q. Recent progress on PEDOT:PSS based polymer blends and composites for flexible electronics and thermoelectric devices. *Mater. Chem. Front.* **4**, 3130–3152 (2020).
2. Novoselov, K. S. *et al.* Electric field effect in atomically thin carbon films. *Gene Expr. Genes Action* **306**, 666–669 (2004).
3. Cheng, L. *et al.* 2D nanomaterials for cancer theranostic applications. *Adv. Mater.* **32**, 1902333 (2020).
4. Zhang, H., Chhowalla, M. & Liu, Z. 2D nanomaterials: Graphene and transition metal dichalcogenides. *Chem. Soc. Rev.* **47**, 3015–3017 (2018).
5. Vilian, A. T. E. *et al.* Recent advances in molybdenum disulfide-based electrode materials for electroanalytical applications. *Microchim. Acta* **186**, 203 (2019).
6. Khan, A. H. *et al.* Two-dimensional (2D) nanomaterials towards electrochemical nanoarchitectonics in energy-related applications. *Bull. Chem. Soc. Jpn.* **90**, 627–648 (2017).
7. Yin, A., Wei, X., Cao, Y. & Li, H. High-quality molybdenum disulfide nanosheets with 3D structure for electrochemical sensing. *Appl. Surf. Sci.* **385**, 63–71 (2016).
8. Chhowalla, M. *et al.* The chemistry of two-dimensional layered transition metal dichalcogenide nanosheets. *Nat. Chem.* **5**(4), 263–275 (2013).
9. Sinha, A. *et al.* MoS2 nanostructures for electrochemical sensing of multidisciplinary targets: A review. *TrAC Trends Anal. Chem.* **102**, 75–90 (2018).
10. Sookhakian, M., Basirun, W. J., Goh, B. T., Woi, P. M. & Alias, Y. Molybdenum disulfide nanosheet decorated with silver nanoparticles for selective detection of dopamine. *Colloids Surf. B Biointerfaces* **176**, 80–86 (2019).
11. Maulik, S., Basu, S., Kanakamedala, K. & Daniels-Race, T. A review of atomic scale characterization techniques of molybdenum disulfide (MoS2). *J. Electron. Mater.* **48**, 3451–3458 (2019).
12. Parra-Alfambra, A. M. *et al.* MoS2 nanosheets for improving analytical performance of lactate biosensors. *Sensors Actuators B Chem.* **274**, 310–317 (2018).
13. Velmurugan, S. & Yang, T. C. K. Fabrication of high-performance molybdenum disulfide-graphitic carbon nitride p-n heterojunction stabilized rGO/ITO photoelectrode for photoelectrochemical determination of dopamine. *ACS Appl. Electron. Mater.* **2**, 2845–2856 (2020).
14. Cheng, M., Zhang, X., Wang, M., Huang, H. & Ma, J. A facile electrochemical sensor based on well-dispersed graphene-molybdenum disulfide modified electrode for highly sensitive detection of dopamine. *J. Electroanal. Chem.* **786**, 1–7 (2017).
15. Guo, X. *et al.* Simultaneous electrochemical determination of dopamine and uric acid based on MoS2nanoflowers-graphene/ITO electrode. *Microchem. J.* **154**, 104527 (2020).
16. Shin, J. W., Yoon, J., Shin, M. & Choi, J. W. Electrochemical dopamine biosensor composed of silver encapsulated MoS 2 hybrid nanoparticle. *Biotechnol. Bioprocess Eng.* **24**, 135–144 (2019).
17. Zribi, R. *et al.* Simultaneous and selective determination of dopamine and tyrosine in the presence of uric acid with 2D-MoS2 nanosheets modified screen-printed carbon electrodes. *FlatChem* **24**, 100187 (2020).
18. Rowley-Neale, S. J., Smith, G. C. & Banks, C. E. Mass-producible 2D-MoS2-impregnated screen-printed electrodes that demonstrate efficient electrocatalysis toward the oxygen reduction reaction. *ACS Appl. Mater. Interfaces* **9**, 22539–22548 (2017).
19. Eslamian, M. & Soltani-Kordshuli, F. Development of multiple-droplet drop-casting method for the fabrication of coatings and thin solid films. *J. Coatings Technol. Res.* **15**, 271–280 (2018).
20. Sreekumar, K. & Bindhu, B. Aqueous exfoliation of molybdenum disulfide using ultrasonication. *Mater. Today Proc.* **5**, 13152–13156 (2018).

21. Sim, D. M. *et al.* Long-term stable 2H-MoS 2 dispersion: Critical role of solvent for simultaneous phase restoration and surface functionalization of liquid-exfoliated MoS 2. *ACS Omega* **2**, 4678–4687 (2017).
22. Ghasemi, F. & Mohajerzadeh, S. Sequential solvent exchange method for controlled exfoliation of MoS2 suitable for phototransistor fabrication. *ACS Appl. Mater. Interfaces* **8**, 31179–31191 (2016).
23. Zhang, Y. *et al.* Ink formulation, scalable applications and challenging perspectives of screen printing for emerging printed microelectronics. *J. Energy Chem.* **63**, 498–513 (2021).
24. Hong, H., Jiyong, H., Moon, K. S., Yan, X. & Wong, C. Rheological properties and screen printability of UV curable conductive ink for flexible and washable E-textiles. *J. Mater. Sci. Technol.* **67**, 145–155 (2021).
25. Faddoul, R., Reverdy-Bruas, N. & Blayo, A. Formulation and screen printing of water based conductive flake silver pastes onto green ceramic tapes for electronic applications. *Mater. Sci. Eng. Solid State Mater. Adv. Technol.* **177**, 1053–1066 (2012).
26. Wang, H., Guo, T., Zhang, Y., Zhang, Q. & Li, H. Rheological properties, antimicrobial activity and screen-printing performance of chitosan-pigment (FeO(OH)·xH2O) composite edible ink. *Prog. Org. Coatings* **111**, 75–82 (2017).
27. Busch, A. *et al.* Rheological characterization of polyanionic cellulose solutions with application to drilling fluids and cuttings transport modeling. *Appl. Rheol.* **28**, 1–17 (2018).
28. Durairaj, R., Mallik, S., Seman, A., Marks, A. & Ekere, N. N. Rheological characterisation of solder pastes and isotropic conductive adhesives used for flip-chip assembly. *J. Mater. Process. Technol.* **209**, 3923–3930 (2009).
29. Liu, L., Shen, Z., Zhang, X. & Ma, H. Highly conductive graphene/carbon black screen printing inks for flexible electronics. *J. Colloid Interface Sci.* **582**, 12–21 (2021).
30. Su, S. *et al.* A molybdenum disulfide@Methylene Blue nanohybrid for electrochemical determination of microRNA-21, dopamine and uric acid. *Microchim. Acta* **186**, 607 (2019).
31. Pramoda, K., Moses, K., Maitra, U. & Rao, C. N. R. Superior performance of a MoS2-RGO composite and a borocarbonitride in the electrochemical detection of dopamine Uric Acid and Adenine. *Electroanalysis* **27**, 1892–1898 (2015).
32. Zhang, X. *et al.* Fabrication of 3D Ni/NiO/MoS2/rGO foam for enhancing sensing performance. *New J. Chem.* **45**, 4387–4392 (2021).
33. Ma, G., Xu, H., Xu, F. & Wang, L. Growth of worm-like and flower-like molybdenum disulfide on graphene nanosheets for sensitive determination of dopamine. *Int. J. Electrochem. Sci.* **12**, 7365–7376 (2017).
34. Kumar, M., Wang, M., Kumara Swamy, B. E., Praveen, M. & Zhao, W. Poly (alanine)/NaOH/ MoS2/MWCNTs modified carbon paste electrode for simultaneous detection of dopamine, ascorbic acid, serotonin and guanine. *Colloids Surf. B Biointerfaces* **196**, 111299 (2020).
35. Zou, H. L., Li, B. L., Luo, H. Q. & Li, N. B. 0D–2D heterostructures of Au nanoparticles and layered MoS2 for simultaneous detections of dopamine, ascorbic acid, uric acid, and nitrite. *Sensors Actuators B Chem.* **253**, 352–360 (2017).
36. Chen, H., Chen, H. & Hong, R. Fabrication of au nanoparticle-decorated mos2 nanoslices as efficient electrocatalysts for electrochemical detection of dopamine. *Catalysts* **9**, 653 (2019).
37. Yue, H. Y. *et al.* Golf ball-like MoS2 nanosheet arrays anchored onto carbon nanofibers for electrochemical detection of dopamine. *Microchim. Acta* **186**, 378 (2019).
38. Zhao, Y. *et al.* In-situ growth of gold nanoparticles on a 3D-network consisting of a MoS2/rGO nanocomposite for simultaneous voltammetric determination of ascorbic acid, dopamine and uric acid. *Microchim. Acta* **186**, 1–10 (2019).
39. Zhu, Z., Jin, C., Miao, X. & Shen, Y. Simultaneous determination of dopamine and uric acid on a MoS2-CPtNPs nanocomposite-modified electrode. *Int. J. Electrochem. Sci.* **15**, 3969–3979 (2020).
40. Sabar, M. *et al.* Fabrication of MoS2 enwrapped carbon cloth as electrochemical probe for non-enzymatic detection of dopamine. *Mater. Lett.* **308**, 131233 (2022).
41. Li, Y., Lin, H., Peng, H., Qi, R. & Luo, C. A glassy carbon electrode modified with MoS2 nanosheets and poly(3,4-ethylenedioxythiophene) for simultaneous electrochemical detection of ascorbic acid, dopamine and uric acid. *Microchim. Acta* **183**, 2517–2523 (2016).
42. Rubio-Govea, R. *et al.* MoS2 nanostructured materials for electrode modification in the development of a laccase based amperometric biosensor for non-invasive dopamine detection. *Microchem. J.* **155**, 104792 (2020).
43. Lei, Y. *et al.* Single-atom doping of MoS2with manganese enables ultrasensitive detection of dopamine: Experimental and computational approach. *Sci. Adv.* **6**, 1–10 (2020).
44. Zhang, Y. *et al.* Electrogenerated chemiluminescence of Ru(bpy)32+ at MoS2 nanosheets modified electrode and its application in the sensitive detection of dopamine. *Spectrochim. Acta Part A Mol. Biomol. Spectrosc.* **240**, 118607 (2020).
45. Sun, H. *et al.* Gold nanoparticle-decorated MoS2 nanosheets for simultaneous detection of ascorbic acid, dopamine and uric acid. *RSC Adv.* **4**, 27625–27629 (2014).
46. Mani, V., Govindasamy, M., Chen, S. M., Karthik, R. & Huang, S. T. Determination of dopamine using a glassy carbon electrode modified with a graphene and carbon nanotube hybrid decorated with molybdenum disulfide flowers. *Microchim. Acta* **183**, 2267–2275 (2016).
47. Arya Nair, J. S., Saisree, S., Aswathi, R. & Sandhya, K. Y. Ultra-selective and real-time detection of dopamine using molybdenum disulphide decorated graphene-based electrochemical biosensor. *Sensors Actuators B Chem.* **354**, 131254 (2022).

Acknowledgements

The authors would like to thank the Slovak Grant Agency for financial assistance, projects VEGA 1/0488/19 and VEGA 1/0602/19. The authors would like to acknowledge financial support from the Slovak Research and Development Agency APVV 17–0300. This article was written thanks to the generous support under the Operational Program Integrated Infrastructure for the project: "Strategic research in the field of SMART monitoring, treatment and preventive protection against coronavirus (SARS-CoV-2)", Project no. 313011ASS8, co-financed by the European Regional Development Fund.

Author contributions

M.P. performed the majority of the experiments. M.H. and M.K. helped with the characterization of dispersions and printed layers. L.L. and J.T. performed electrochemical measurements. M.P. and L.L. wrote the manuscript. P.G. supervised the project and characterized electrodes using SEM/EDS. All authors discussed and revised the manuscript.

Competing interests

The authors declare no competing interests.

Additional information

Supplementary Information The online version contains supplementary material available at https://doi.org/10.1038/s41598-022-16187-2.

Correspondence and requests for materials should be addressed to P.G.

Reprints and permissions information is available at www.nature.com/reprints.

Publisher's note Springer Nature remains neutral with regard to jurisdictional claims in published maps and institutional affiliations.